# Evaluation of Methodology for Lightning Impulse Voltage Distribution over High-Voltage Windings of Inductive Voltage Transformers

Bojan Trkulja [1,†], Ana Drandić [1,*,†] , Viktor Milardić [1] and Igor Žiger [2]

1 Faculty of Electrical Engineering and Computing, University of Zagreb, Unska 3, 10000 Zagreb, Croatia; bojan.trkulja@fer.hr (B.T.); viktor.milardic@fer.hr (V.M.)
2 Končar Instrument Transformers Inc., Ulica Josipa Mokrovića 10, 10000 Zagreb, Croatia; igor.ziger@koncar-mjt.hr
* Correspondence: ana.drandic@fer.hr
† These authors contributed equally to this work.

**Abstract:** Knowledge of lightning impulse (LI) voltage distribution over transformer windings during the design stage of the transformer is very important. Specific design differences in inductive voltage transformers make the transient analysis approach different to the approach to the power transformers. In this paper, a methodology for acquiring lightning impulse voltage distribution over high-voltage (HV) winding of inductive voltage transformers is presented and evaluated. Resistance, inductance, and capacitance matrices are calculated using the integral and boundary element methods (BEM) approach. Additionally, in order to improve the capacitance matrix solver, adaptive cross approximation (ACA) is applied. These parameters are then used to solve the equivalent circuit model in time domain. In order to evaluate the methodology, an experimental and numerical investigation of the layer discretisation, iron core influence, and accuracy of the proposed methodology is performed. The comparison of numerical results with measurements confirms the validity of the methodology.

**Keywords:** lightning impulse testing; core influence; voltage transformers; numerical simulation; adaptive cross-approximation

## 1. Introduction

Voltage transformers are built for decades-long operation in the electric power system. During their operation, they are subjected to high-voltage and high-frequency stresses. Due to this, they have to pass standardized tests and satisfy specific requirements before being put into operation in the power system. One of these tests is the lightning impulse (LI) test that determines transformers' ability to withstand transient overvoltages. Due to the devastating effect that transient overvoltages can have on transformers, such as insulation breakdown, it is very helpful and important to have an accurate simulation of the LI test during the transformer design process. A transient analysis of distribution and power transformers can be found in various papers [1–10], while there are a lack of papers on instrument transformers [11,12]. Due to their specific design, it is of great value to investigate transient analysis of voltage transformers.

The transformer winding models used for transient studies can be placed into three categories: white-box models [3,11,13], grey-box models [7,14], and black-box models [15]. White-box models can be solved using lumped-parameter [5], a multiconductor transmission line (MTL) [13], and hybrid approaches. A good analysis of different transformer winding models for transient studies can be found in [16]. In this paper, the methodology with a white-box model that can be used by transformer manufacturers to optimise insulation during the design of inductive voltage transformer is presented and evaluated. Dommel's approach is used for the LI-test simulation [17]. Since this approach requires

lumped parameters, self-developed solvers for the calculation of resistance (R), inductance (L), and capacitance (C) parameters are used. The accuracy of the lighting impulse modeling approach can be found in previous publication [11], where it was confirmed by measurements. This paper is an extension of the authors' investigation of the impulse response in voltage transformers. In this paper, the authors expand their investigation and present and evaluate a methodology for acquiring LI voltage distribution over the high-voltage (HV) winding of inductive voltage transformers. The utilization of other methods and methodologies proved not to be achievable in a reasonable timeframe for inductive voltage transformers. This is due to the coil shape and a high number of winding turns, which results in a model that consists of a relatively large number of elements. This also requires a brief analysis of the discretisation of layers for the inductive voltage transformer that was used for investigation, since it has a direct influence on the existence of the voltage oscillations between winding turns in numerical simulations, which are needed to determine the possibly dangerous overvoltages.

During the lighting impulse test, the low voltage (LV) coil is short-circuited and the influence of the magnetic core is assumed to be negligible in many inductance models used for transient analysis. This is due to the fact that, when the LV coil is short-circuited, the currents produce a magnetic flux in the core that opposes the main flux, leaving a negligible amount of flux in the core. Since this could influence the accuracy of the simulation, one of the objectives of this work is an experimental investigation of core influence to fully validate our methodology. Moreover, in this work, we focus on the distribution of voltages between different turns. An investigation into core influence carried out done by the experimental method. An investigation into the influence of iron core on lighting impulse distribution in a power transformer winding can be found in [18]. Additionally, due to the fact that capacitance matrix calculation, which is based on the boundary element method (BEM), has huge computational and memory requirements, we also introduce the use of adaptive cross-approximation (ACA) [19–21] to solve the problem more efficiently.

The importance of the presented work is, therefore, two-fold: it presents the complete methodology for LI voltage distribution of inductive voltage transformers that can be used by engineers for a transformer winding insulation design that is based on the lumped parameter approach and made more efficient by the implementation of the ACA algorithm, and, during the evaluation of said methodology, confirms the negligible influence of transformer iron core on lighting impulse voltage distribution and investigates the necessary layer discretisation when modelling the HV winding of inductive voltage transformers.

This paper is organized in the following order: In Section 2, the theoretical background of the experimental and numerical methods used to obtain the lighting impulse distribution is presented. In Section 3 the methodology is evaluated, including the experimental investigation of transformer core influence on LI distribution over HV windings of an inductive voltage transformer, analysis of layer discretisation, the comparison of simulated results to measurements, along with the analysis of the benefit of using ACA during the capacitance matrix calculation. Finally, the conclusion of this work is presented in Section 4.

## 2. Theoretical and Experimental Methods

Calculation of impulse voltage distribution depends on knowledge of dimensions of coils and turns, as well as knowledge of materials and dielectric parameters. The computational modelling approach can be used to obtain LI voltage distribution during the design phase and simulation of this phenomenon. There are a few steps that have to be taken in order to obtain the LI voltage distribution over HV windings of an inductive transformer. Firstly, when using the proposed methodology, the geometry of the transformer has to be known, as this is the input for all calculations. Winding configuration is taken into account with the use of a topological matrix. Use of the topological matrix and the detailed modeling of the winding allow for different transformer winding configurations to be addressed using the presented methodology. Next, the problem must be properly discretised to gain accurate results. LI voltage distribution in this paper is obtained using a

transient solver, which is based on Dommel's approach. This approach requires knowledge of RLC matrices, so the third step would be their calculation. Block scheme that shows the steps of the proposed methodology for LI voltage distribution is presented in Figure 1. In practice, the steps of the presented methodology would be repeated until the desired optimisation of insulation regarding transient overvoltages is reached.
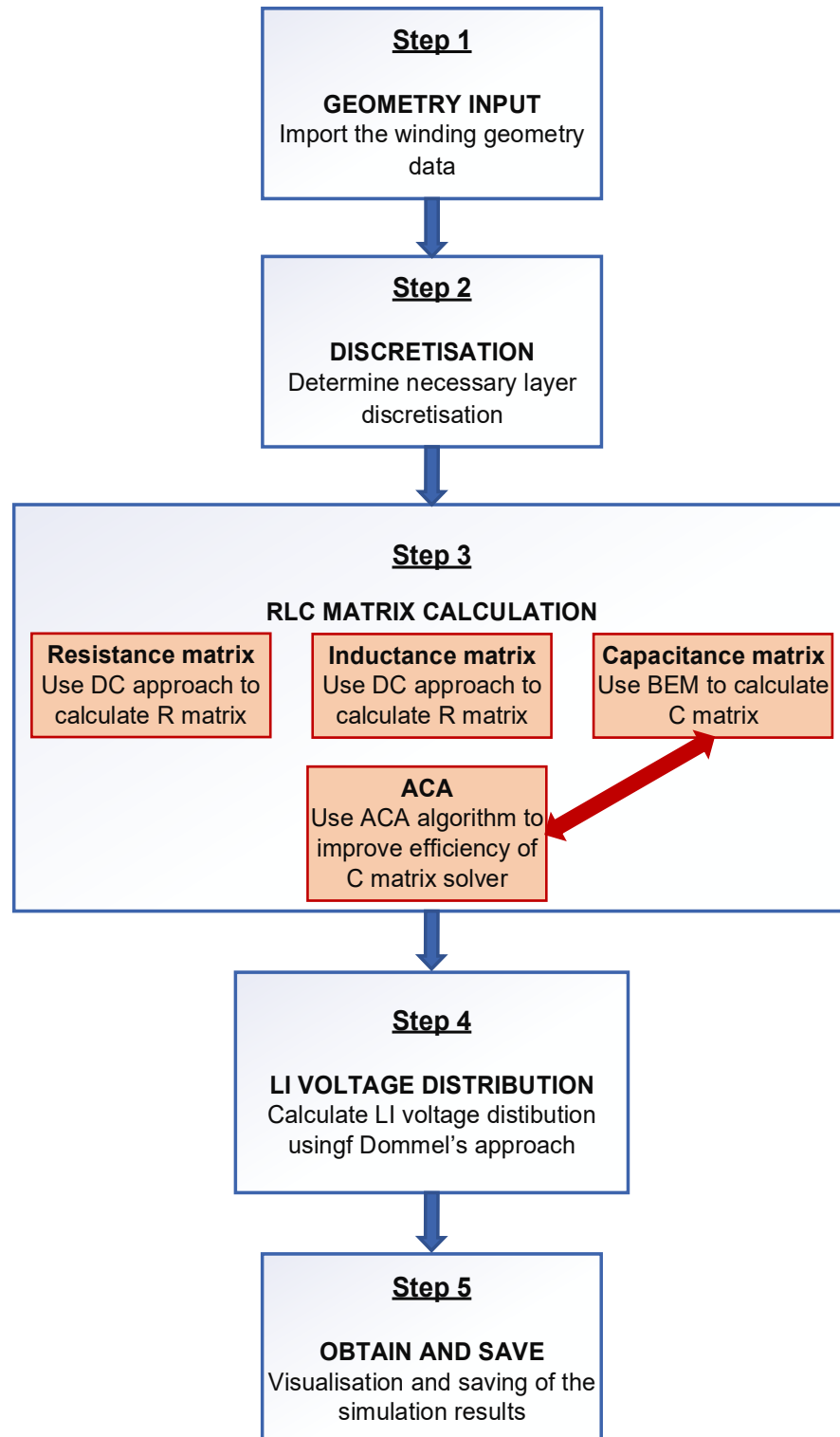


**Figure 1.** Flowchart of steps for the simulation of lightning impulse (LI) voltage distribution.

This section provides background for both the theoretical and experimental methods used to obtain and evaluate the simulation of LI voltage distribution over HV windings of inductive voltage transformers.

### 2.1. Method for Voltage Distribution Simulation in Time Domain

A method for the calculation of the lightning impulse voltage distribution was developed, used, and published in the past [11,17]. Therefore, only a brief summary of the method is given in this section. All inductive and capacitive couplings, as well as turn resistances, are taken into account. As an example, a three-turn equivalent circuit of a transformer coil is shown in Figure 2. As previously mentioned, a solver based on Dommel's method was developed to obtain the results of LI voltage distribution over HV windings of inductive voltage transformers. Dommel's method replaces the inductances and capacitances of the equivalent circuit with resistances and current sources. Unknown voltages are computed in time steps $\Delta t$ using the following algebraic equations:

$$\mathbf{G} = \mathbf{D}^T \left(\mathbf{R} + \frac{2}{\Delta t}\mathbf{L}\right)^{-1}\mathbf{D} + \frac{2}{\Delta t}\mathbf{C}, \tag{1}$$

$$\mathbf{i_{RL}}(t) = \left(\mathbf{R} + \frac{2}{\Delta t}\mathbf{L}\right)^{-1}\mathbf{Du}(t) + \mathbf{I_{RL}}(t - \Delta t), \tag{2}$$

$$\mathbf{i_C}(t) = \frac{2}{\Delta t}\mathbf{Cu}(t) + \mathbf{I_C}(t - \Delta t), \tag{3}$$

$$\mathbf{I_{RL}}(t - \Delta t) = \left(\mathbf{R} + \frac{2}{\Delta t}\mathbf{L}\right)^{-1}\left[\left(\frac{2}{\Delta t}\mathbf{L} - \mathbf{R}\right)\mathbf{i_{RL}}(t - \Delta t) + \mathbf{Du}(t - \Delta t)\right], \tag{4}$$

$$\mathbf{I_C}(t - \Delta t) = -\mathbf{i_C}(t - \Delta t) - \frac{2}{\Delta t}\mathbf{Cu}(t - \Delta t), \tag{5}$$

$$\mathbf{I} = \mathbf{D}^T\mathbf{I_{RL}}(t - \Delta t) + \mathbf{I_C}(t - \Delta t), \tag{6}$$

$$\mathbf{Gu}(t) = \mathbf{i}(t) - \mathbf{I} \tag{7}$$

where $\mathbf{D}$ is the topological matrix, $\mathbf{G}$ is the nodal conductance matrix, $\mathbf{i_{RL}}(t), \mathbf{i_C}(t), \mathbf{I_{RL}}(t - \Delta t), \mathbf{I_C}(t - \Delta t)$ are the current vectors of the equivalent current sources, $\mathbf{u}(t)$ is the node voltage in $t$, and $\mathbf{I}$ is the injected node current vector.
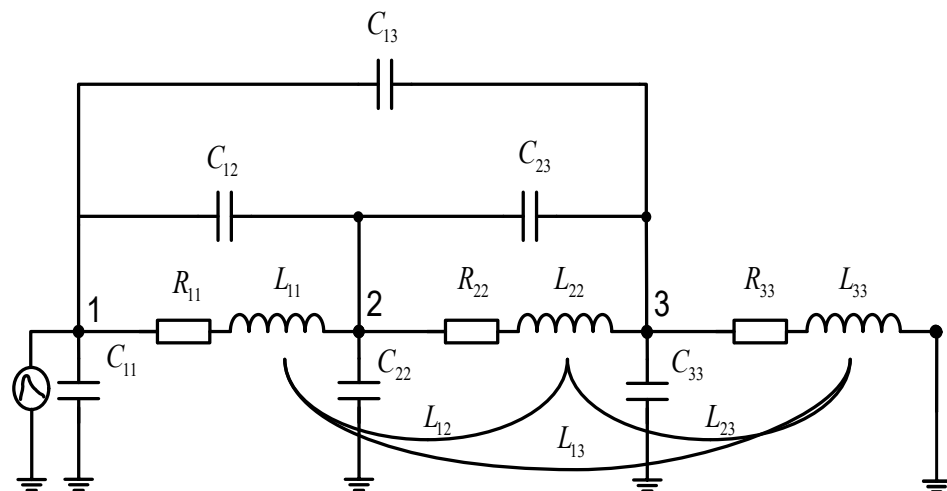


**Figure 2.** Equivalent circuit of a three-turn transformer coil.

### 2.2. Inductance Matrix Calculation

The method for the calculation of inductance matrix is based on the method for calculating inductances of coaxial circular coils with a rectangular cross-section and uniform current densities in the air, published in [22]. This method is proven to have very fast calculations that yield accurate inductance values. The iron core influence on the inductance values is assumed to be negligible due to the fact that the secondary winding is short-circuited. The correctness of this assumption is proven in Section 3.

### 2.3. Resistance Matrix Calculation

The high-voltage winding of a voltage transformer can consist of tens of thousands of turns, which means that turns in the winding model have to be grouped. This means that turns can be simulated as solid thick conductors that behave as a stranded coil in which the current density is uniform. Skin and proximity effects are practically negligible, and DC calculation is used to obtain the resistance matrix.

### 2.4. Capacitance Matrix Calculation

The calculation of capacitance values is based on an approximation of the charge density on transformer winding. Since, in this paper, ACA is used to improve the capacitance matrix solver, for completion of the paper, the method of capacitance matrix calculation is explained in more detail in this subsection. A two-dimensional approximation is used. Using the 2D Green function, the electric field potential phasor at any point $\vec{r}$ can be found using equation [23,24]:

$$\varphi(\vec{r}) - \int_l \sigma(\vec{r}')G(\vec{r},\vec{r}')\mathrm{d}S', \tag{8}$$

where $\sigma(\vec{r}')$ is the unknown surface charge density and $G(\vec{r},\vec{r}')$ is the Green's function of the Laplace electrostatic problem:

$$G(\vec{r},\vec{r}') = \frac{1}{4\pi|\vec{r}-\vec{r}'|}. \tag{9}$$

Surface charge density on each segment $i$ can be approximated with:

$$\sigma_i = \sum_{k=1}^{K} \alpha_{ik} f_k \tag{10}$$

In Equation (10), $K$ is the number of basis functions and $\alpha_{ik}$ are the unknown coefficients that need to be computed. The simplest approach with constant basis functions is implemented, which means that $K = 1$. Now, combining Equations (8)–(10), potential can be calculated using:

$$\varphi(\vec{r}) = \sum_{i=1}^{N} \alpha_i \int f_1 \frac{1}{4\pi|\vec{r}-\vec{r}'|}\mathrm{d}S. \tag{11}$$

Unknown coefficients $\alpha_i$ are obtained by solving the linear system of equations:

$$\mathbf{A}\alpha_i = \mathbf{B} \tag{12}$$

where $\mathbf{B}$ is the matrix of known potentials, and $\mathbf{A}$ is the system matrix formed using Equation (8).

When the unknown linear charge density is obtained, it is possible to calculate the capacitance matrix of the windings. This is done using following equations:

$$C_{ij} = \frac{Q_{ij}}{\varphi_i - \varphi_j}, i \neq j, \tag{13}$$

and:

$$C_{ii} = \frac{Q_{ii}}{\varphi_i}. \tag{14}$$

Here, $\varphi_i$ and $\varphi_j$ are potentials of the $i$-th and $j$-th conductor, and $Q_{ij}$ is the total charge on the $j$-th conductor influenced by the charge on the $i$-th conductor:

$$Q_{ij} = \int_{S_j} \sigma dS_j = \sum_{k=1}^{N_j} \sigma_{kj} S_{kj}. \tag{15}$$

Here, $\sigma_{kj}$ is the surface charge density on the $k$-th segment of the $j$-th conductor, $N_j$ is the number of segments on the $j$-th conductor, and $S_{kj}$ is the surface of the $k$-th segment of the $j$-th conductor.

It is important to note that the charge conservation law was not met with previous equations and, in order to satisfy it, equation:

$$\sum_{i=1}^{N} Q_i = 0 \tag{16}$$

is added to the system of equations in Equation (12).

### 2.5. Adaptive Cross-Approximation

Since the memory requirements and computational costs of BEM rise quadratically with the number of unknowns, different acceleration techniques have been developed over the years. One such technique is adaptive cross-approximation (ACA) [19–21]. This section will provide a brief description of the ACA algorithm used to improve the BEM solver for capacitance matrix calculation. The implementation and efficiency of the ACA algorithm for different problems can be found in [25–31].

ACA algorithm approximates the system matrix by lower rank matrices. The idea is that only certain elements of the matrix have to be computed, while the rest of the matrix is approximated with a specified error tolerance. It is important to note that ACA is an algebraic method, meaning that it is not necessary to know the integral equation function, fundamental functions, and the equation formulation. There are two implementations of the ACA algorithm, a fully pivoted ACA, and partially pivoted ACA. While fully pivoted implementation requires full knowledge of the system matrix, partially pivoted implementation of the algorithm only requires the calculation of specific entries of the system matrix. In this paper, all results are obtained using the partially pivoted ACA algorithm, based on the works in [31–33].

Before employing the ACA algorithm, it is important to obtain a hierarchical representation of the matrix. This can be done by the recursive division of the matrix into blocks using geometrical clustering. The next step is the determination of admissible and non-admissible blocks. Admissible blocks can be approximated by low-rank matrices, while non-admissible blocks have to be explicitly computed. The admissibility of the blocks is determined using the admissibility criterion, defined as:

$$\left| i_x - i_y \right| \geq \mu \quad \&\& \quad \left| y_x - y_y \right| \geq \mu, \quad \mu > 0, \tag{17}$$

where $\mu$ is an arbitrary parameter, and $(i, j)$ are cell indices when a background grid is applied. More information on this type of admission criterion can be found in [29].

As previously mentioned, the goal is to approximate the system matrix by lower-rank matrices and for a known error tolerance. Block $\mathbf{A}^{mxn}$ can be approximated by approximation matrix $\tilde{\mathbf{A}}^{mxn}$ and the residual matrix $\mathbf{R}^{mxn}$:

$$\mathbf{A}^{mxn} = \tilde{\mathbf{A}}^{mxn} + \mathbf{R}^{mxn}. \tag{18}$$

The approximated matrix $\tilde{\mathbf{A}}^{mxn}$ consists of the lower rank matrices $\mathbf{U}^{m \times r}$ and $\mathbf{V}^{n \times r^T}$:

$$\tilde{\mathbf{A}}^{mxn} = \mathbf{U}^{m \times r} \mathbf{V}^{n \times r^T} = \sum_{k=1}^{r} \mathbf{u}_k^{m \times 1} \mathbf{v}_k^{n \times 1^T}. \tag{19}$$

The stopping criterion of the ACA algorithm is:

$$\|\mathbf{R}^{mxn}\|_F \leq \varepsilon \|\mathbf{A}^{mxn}\|_F, \tag{20}$$

where $\varepsilon$ is a previously specified error tolerance. The stopping criterion in Equation (20) allows for the adaptive determination of approximated matrix rank. The main steps of the ACA algorithm are [30]:

- Initialization:
  $\hat{A}_0 = 0; i_0 = 1$
- Iterations or $k = 0, 1, 2, \ldots$:
  - Residual matrix row and pivoted column determination
    $row = e_{i_{k+1}}^T A$
    $R_k^T e_{i_{k+1}} = row - \sum_{l=1}^{k} (u_l)_{i_{k+1}} v_l^T$
    $j_{k+1} = max \left| (R_k)_{i_{k+1},j} \right|$
  - Residual matrix row and column calculation
    $v_{k+1} = \dfrac{R_k^T e_{i_{k+1}}}{(R_k)_{i_{k+1},j_{k+1}}}$
    $u_{k+1} = A e_{i_{k+1}} - \sum_{l=1}^{k} (v_l)_{j_{k+1}} u_l$
  - Then, pivot determination and approximation update
    $i_{k+2} = max |(u_{k+1})_i|$
    $\hat{A}_{k+1} = \hat{A}_k + u_{k+1} v_{k+1}^T$
- Stopping criterion check.

When ACA algorithm is used, the linear system of equations in Equation (12) becomes:

$$\mathbf{U}^{m \times r} \mathbf{V}^{n \times r^T} \boldsymbol{\alpha} = \mathbf{B}. \tag{21}$$

The system of equations in Equation (21) has a reduced number of operations compared to the system in Equation (12), and is solved using the generalized minimal residual method (GMRES) [34].

Since, in this paper, a partially pivoted ACA algorithm is implemented, which does not compute the whole system matrix, a small modification of the stopping criterion is used:

$$\|\mathbf{u}_k\|_F \|\mathbf{v}_k\|_F \leq \varepsilon \|\tilde{\mathbf{A}}_k\|_F. \tag{22}$$

The norm of the matrix $\|\tilde{\mathbf{A}}_k\|_F$ can be recursively acquired using the following equation:

$$\|\tilde{\mathbf{A}}_k\|_F^2 = \|\tilde{\mathbf{A}}_{k-1}\|_F^2 + \|\mathbf{u}_k\|_F^2 \|\mathbf{v}_k\|_F^2 + 2 \sum_{p=1}^{k-1} \mathbf{u}_k^T \mathbf{u}_p \mathbf{v}_k \mathbf{v}_p^T. \tag{23}$$

*2.6. Experimental Setup*

For measurements, an impulse generator, as in [11], was used for generation of the impulse voltage. The generator is able to produce a 1.2/50 μs voltage waveform in the range of 1–100 kV. Then, oscilloscope LeCroy LT354, 500 MHz, 1 GS/s and probes Tektronix P6015 40 kV 1000:1, 75 MHz, 100 MΩ were used to measure voltage distribution on the HV-winding of the instrument transformer. The electric scheme of the impulse generator and lighting impulse waveform in time domain is shown in Figure 3.
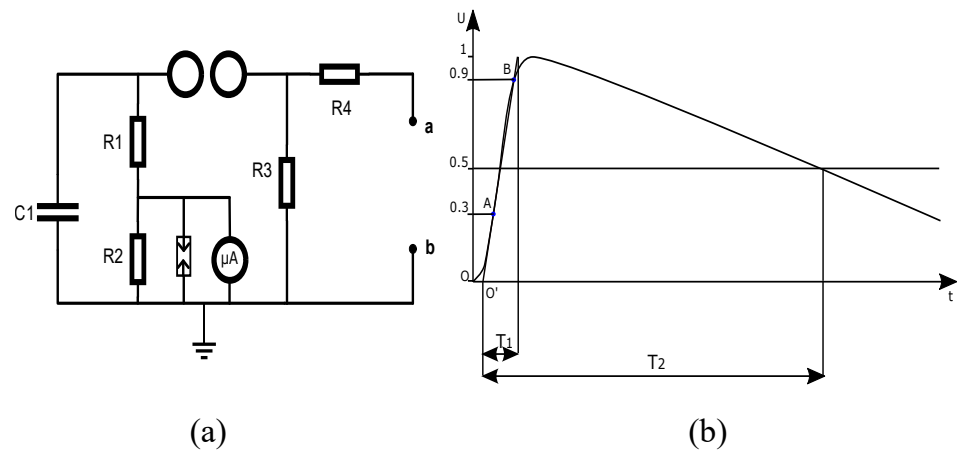
(a)  (b)

**Figure 3.** Impulse generator and generated waveform: (**a**) Electric scheme of the impulse generator. The device under test is connected via terminals a and b; (**b**) Waveform of the standard lighting impulse in the time domain. In accordance with the IEC 60060-1 standard: $T_1$ = 1.2 µs ± 30%, $T_2$ = 50 µs ± 20%.

The voltages at all taps could not be recorded at the same time for one pulse. Two probes were used for each tap. One probe was on the input pulse and the other was on the tap. This also means there were small differences in the input voltages for each tap. Nevertheless, in order to properly verify the results, a simulation was conducted for every input voltage (of the tap measured) and the results are in very good comparison, as presented in Section 3.4.

## 3. Results and Discussion

In order to evaluate the proposed methodology, an investigation of its validity was confucted by comparison with measurements, and on the factors that were recognized as possible influences on the numerical result accuracy. Therefore, the scope of the investigation as follows:

(1) Investigation of transformer core influence on LI voltage distribution due to the fact that, during the inductance matrix calculation this influence was assumed to be negligible;
(2) Investigation of necessary layer discretisation in order to encompass the entire wave phenomenon and achieve satisfactory accuracy;
(3) Verification of the obtained numerical simulation results by comparison with measurements;
(4) Investigation of the improved capacitance matrix calculations when ACA algorithm is implemented.

### 3.1. Instrument Voltage Transformer Used for Investigation

Inductive voltage transformers consist of a magnetic core, primary winding, and one or more secondary windings. In order to perform an experimental investigation, a custom-made instrument transformer active part was acquired. The HV coil has 238 layers with 185 turns which gives a total of 44,030 turns. The dimensions of the active part, depicted in Figure 4, are: length: 450 mm; height: 365 mm; width: 95 mm; diameter of outer winding: 285 mm.

The transformer active part was made with additional taps along the winding to measure voltage and confirm the developed approach. Soldering the taps along the winding leads to some inherent changes, however small. In order to reduce the influence of taps on measurements, the length of tap leads was as short as possible and taps were angularly symmetric along the winding. Since the simulation and measurement results are in good agreement, tap influence can be considered negligible.
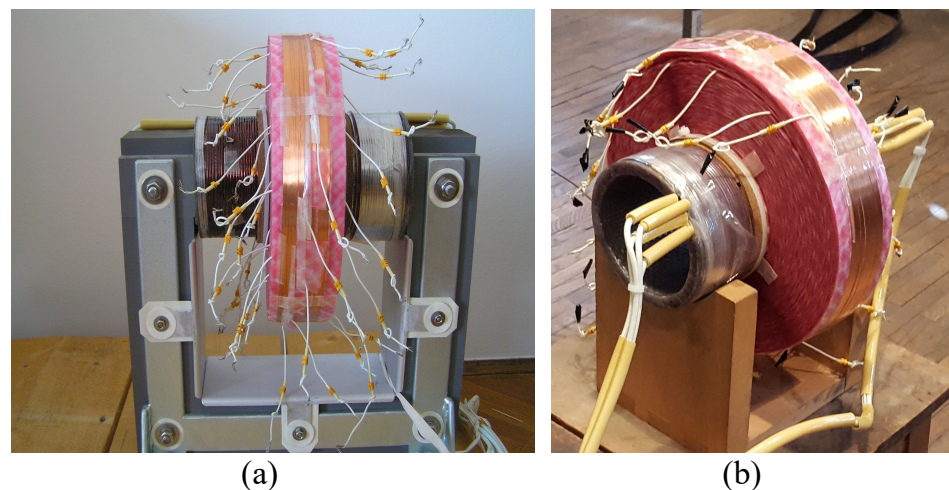
(a)                                                           (b)

**Figure 4.** Active part of the transformer: (**a**) Active part with iron core; (**b**) Active part without core.

### 3.2. Experimental Investigation of Transformer Core Influence on LI Distribution

Measurements were carried out to identify the way the core influences the lighting impulse voltage distribution. The same measurement process was, therefore, performed twice: once on the model with an iron core, and once after the core was removed. Both cases are shown in Figure 3. Firstly, an impulse generator was used to apply the voltage impulse to the primary winding while the secondary winding was short-circuited. Then, the voltage distribution was measured using the oscilloscope.

The voltages between different taps are investigated. A comparison of the measurement results, depicted in Figure 5, shows that LI voltage distribution over the HV winding of the inductive voltage transformer with an iron core is very similar to the distribution without an iron core. Since the capacitance values of windings do not change in these cases, it means that the magnetic flux in the transformer core is canceled out when the LV winding is short-circuited.
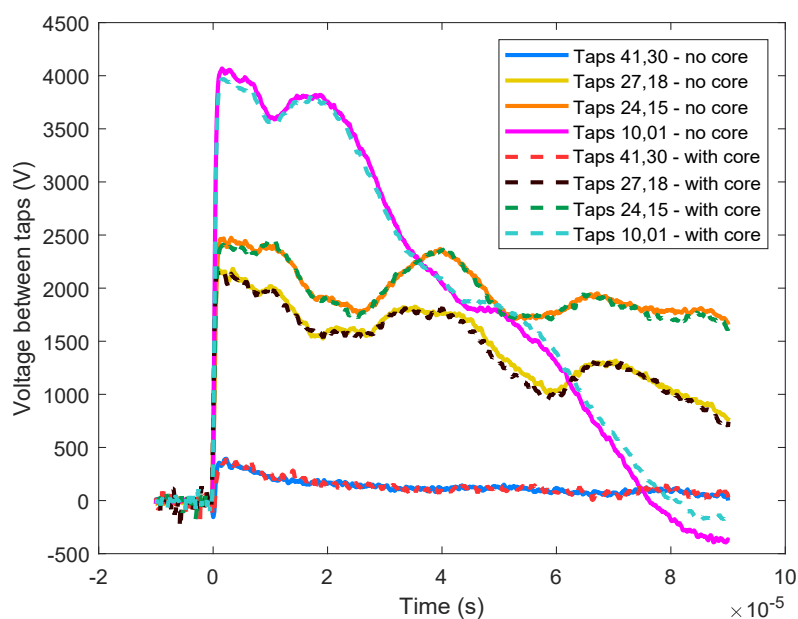


**Figure 5.** Measurement results for voltages between taps with and without iron core.

The results validate the assumption that influence of the magnetic core is negligible during LI-tests when the secondary winding is short-circuited, meaning that the inductance matrix can be calculated using the method for calculating the inductance of coils in the air.

### 3.3. Investigation of Layer Discretisation

Voltage distribution on taps acquired by measurements is presented in Figure 6. Since the transformer under investigation has 238 layers, a simulation with one element per layer, consisting of 185 turns, was made. The distribution of LI voltage on all taps was monitored. The results obtained by numerical simulation when one element per layer was used can be observed in Figure 7.
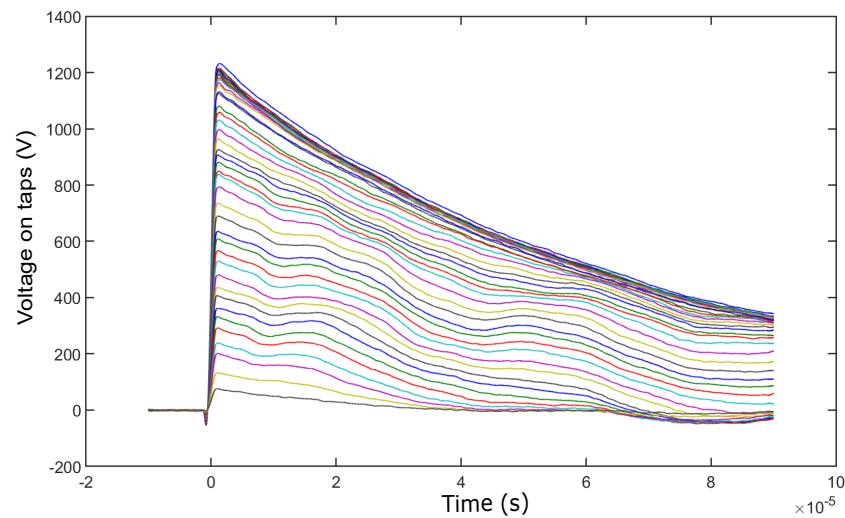


**Figure 6.** LI voltage distribution on taps obtained by measurements.
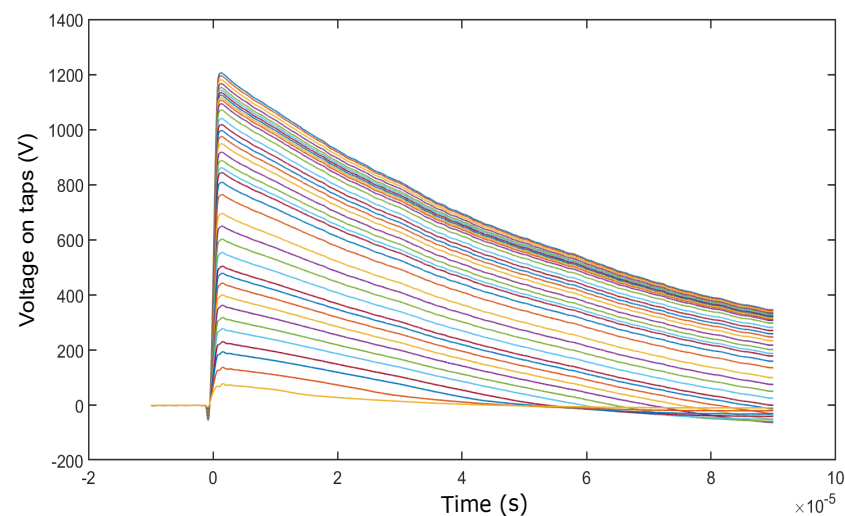


**Figure 7.** LI voltage distribution on taps obtained by simulation with one element per layer.

By comparing the results of calculations and measurements, it can be seen that, to model a layer of 185 turns with one set of concentrated RLC elements, the wave phenomenon present in the measurements is not present in the calculation results. The oscillation that can be observed in the measurement in Figure 6 is completely damped in simulation in Figure 7. The reason for this is that the input wave contains frequencies higher than 1 MHz. Since the wavelength for 100 kHz is $\lambda = 1732$ m, it is assumed that it is necessary to have a maximum of 50 turns in one replacement element, to descend to approximately $0.1\lambda$, and thus ensure that the wave phenomenon visible in measurements will be present in the calculation results. To ensure good accuracy, each layer was modelled with four elements, which led to a total of 952 elements that model the HV winding. The results of LI voltage distribution are presented in Figure 8. This result shows that special care should be taken during the discretisation step when the methodology is used.
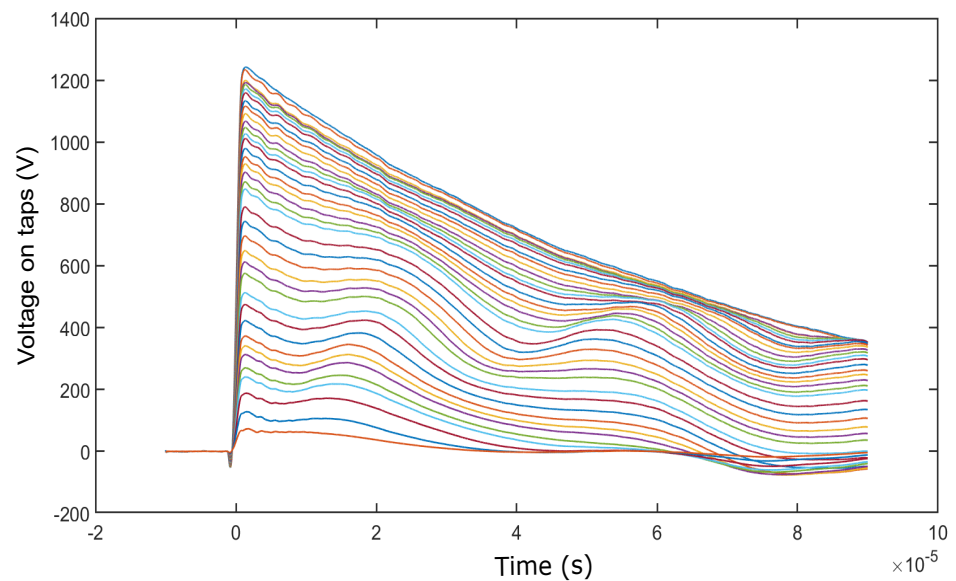
**Figure 8.** LI voltage distribution on taps obtained by simulation with four element per layer.

*3.4. Numerical Simulation Verification*

The numerical results of LI test simulation, obtained by the methodology presented in previous sections, are compared with measurement results. The voltages between different taps are observed. This is important to determine insulation stresses between layers of the winding. As shown in Figure 9, the measurement and simulation results are in agreement, which validates the accuracy of the presented approach. Due to the number of turns of the voltage transformer, each of the 238 layers was modelled, with four elements. Additionally, voltage maximum values observed on different taps are presented in Table 1. The relative error is smaller for the part of the winding on which the most overvoltage stress occurs, while the differences between values at the end of the winding are more pronounced. Nevertheless, the relative error of maximum voltage values does not exceed 4%. Obtained RLC matrices are shown in Figure 10.
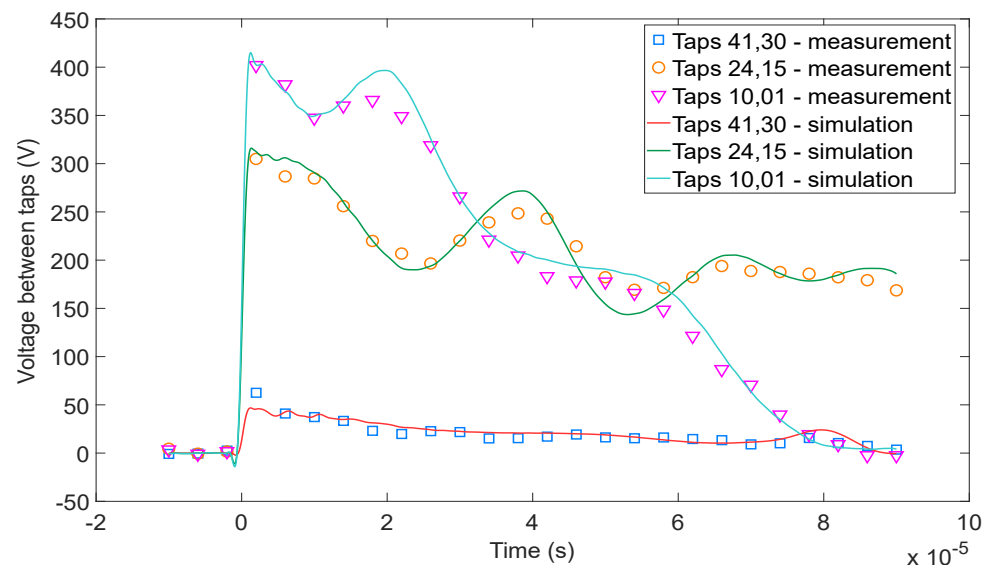


**Figure 9.** Comparison of simulation and measurement results for voltages between taps for the 1.2 kV voltage level.

**Table 1.** Voltage maximum value on different taps obtained by measurements and numerical simulation for the 1.2 kV voltage level.

| | Tap Number | | | | | |
|---|---|---|---|---|---|---|
| | **41** | **30** | **24** | **15** | **10** | **1** |
| maximum voltage— measurements [V] | 1232 | 1165 | 995.8 | 689.1 | 479.2 | 75.32 |
| maximum voltage—simulation | 1234 | 1185 | 1011 | 696.3 | 474.7 | 72.62 |
| relative error [%] | 0.16 | 1.72 | 1.53 | 1.04 | 0.94 | 3.58 |



(a)



(b)
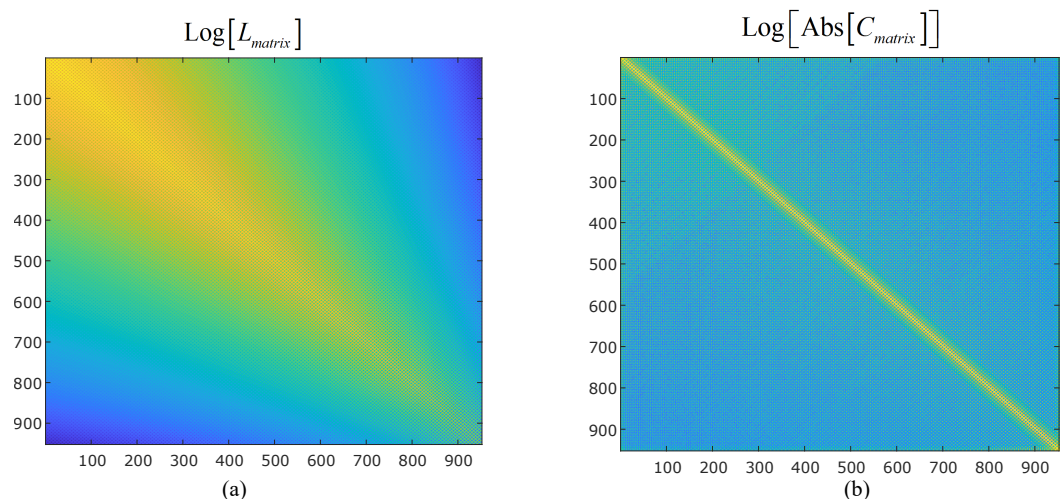
**Figure 10.** Visualization of the calculated LC matrices composed of 952 elements: (**a**) Inductance matrix; (**b**) Capacitance matrix.

### 3.5. Use of the ACA for C Matrix Calculation

The ACA algorithm, explained in Section 2, was implemented to improve the efficiency of the BEM solver used to compute the capacitance matrix. The error tolerance of the ACA is set to $10^{-9}$, while the GMRES iterative solver convergence tolerance is set to $10^{-5}$. Using these tolerances, the relative error for the obtained charge density in the case of BEM-ACA solver, when compared with the BEM solver, is under 0.1%.

As previously mentioned, one of the ACA algorithm advantages is compression of the system matrix. This enables the calculation of larger matrices with existing computational resources. The matrix compression ratio is defined as:

$$CR = \frac{Uncompressed\ size}{Compressed\ size} \tag{24}$$

while space savings can be calculated by:

$$SpaceSavings = \frac{|Uncompressed\ size\text{-}Compressed\ size|}{Compressed\ size} \times 100 \tag{25}$$

The memory consumption of both BEM and BEM-ACA solvers for a different number of discretisation elements is presented in Figure 11. The space savings and compression ratio for the previous example are given in Table 2. The memory requirements of the calculation were considerably reduced, with the implementation of the ACA algorithm. Data from Figure 11 and Table 2 prove the increased efficiency of the solver when the ACA algorithm is implemented. This enables the calculations to be performed on normal computer configurations without the fear of lacking computational resources.
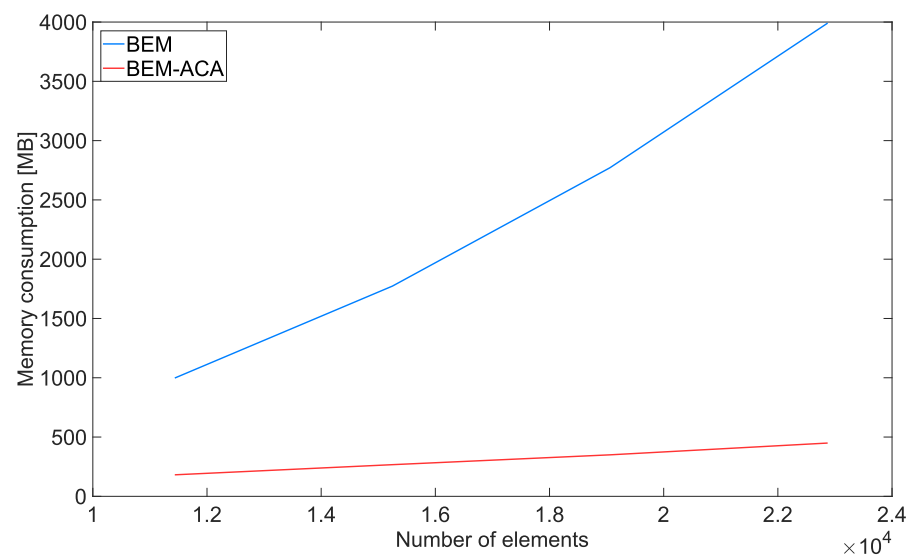
**Figure 11.** System matrix memory consumption for a different number of discretisation elements with BEM solver and with BEM-ACA solver.

**Table 2.** Space savings and matrix compression ratio for different number of discretisation elements.

|  | Number of Elements | | | |
|---|---|---|---|---|
|  | 11,436 | 15,248 | 19,060 | 22,872 |
| **space savings [%]** | 81.80 | 84.94 | 86.65 | 88.76 |
| **compression ratio** | 5.49 | 6.64 | 7.49 | 8.90 |

## 4. Conclusions

This paper presents and evaluates a methodology for acquiring LI voltage distribution over an HV winding of inductive voltage transformers. The presented work is limited to two-dimensions and the simulations and measurements when the secondary side is shorted, since it is standard procedure during the LI transformer tests.

In order to properly evaluate the methodology, both numerical and experimental investigations were made. Since the modelling of voltage instrument transformers requires a reduction in the model in order to obtain a solvable system, an investigation into layer discretisation was made. This investigation emphasizes the importance of the good discretisation of layers in order to obtain good simulation accuracy, since oversimplification of the transformer model regarding the number of elements will lead to discrepancies between the simulation and measured LI voltage distributions. Furthermore, as the assumption that transformer core influence during LI-simulations can be considered negligible, since the shot-circuited secondary winding was used when calculating the inductance matrix, the experimental method was used to investigate this claim, since it could affect the accuracy of simulation results. Finally, the results of the numerical simulation of the presented transformer, with an investigationinto the voltages between the transformer taps, are presented. A comparison between the measurement results and simulated results demonstrates the accuracy of the presented method for LI voltage distribution simulation in voltage transformers. Moreover, it is shown that the additional use of adaptive cross-approximation can significantly improve the capacitance matrix solver, thus making the developed LI-test simulation more efficient. All of these results validate the proposed methodology, which should be of interest to transformer manufacturers, since the purpose of this methodology is for use during the design process of transformers in order to optimise the insulation regarding the transient overvoltages. Further work in this area could include code optimisation, the development of simplified graphical user interface, and analysis of the frequency domain.

## Abbreviations

The following abbreviations are used in this manuscript:

| | |
|---|---|
| HV | high voltage |
| LI | lightning impulse |
| BEM | Boundary element method |
| ACA | Adaptive cross approximation |
| MTL | multiconductor transmission line |
| LV | low voltage |
| R | resistance |
| L | inductance |
| C | capacitance |
| GMRES | Generalized minimal residual method |

## References

1. Popov, M.; Van Der Sluis, L.; Paap, G.C.; De Herdt, H. Computation of very fast transient overvoltages in transformer windings. *IEEE Trans. Power Deliv.* **2003**, *18*, 1268–1274. [CrossRef]
2. Popov, M.; van der Sluis, L.; Smeets, R.; Lopez-Roldan, J.; Terzija, V. Modelling, simulation and measurement of fast transients in transformer windings with consideration of frequency-dependent losses. *IET Electr. Power Appl.* **2006**, *1*, 29–35. [CrossRef]
3. Smajic, J.; Steinmetz, T.; Rüegg, M.; Tanasic, Z.; Obrist, R.; Tepper, J.; Weber, B.; Carlen, M. Simulation and measurement of lightning-impulse voltage distributions over transformer windings. *IEEE Trans. Magn.* **2014**, *50*. [CrossRef]
4. Smajic, J.; Franz, T.; Bucher, M.K.; Limone, A.; Shoory, A.; Skibin, S.; Tepper, J. Computational and Experimental Investigation of Distribution Transformers under Differential and Common Mode Transient Conditions. *IEEE Trans. Magn.* **2017**, *53*. [CrossRef]
5. Župan, T.; Trkulja, B.; Obrist, R.; Franz, T.; Cranganu-Cretu, B.; Smajic, J. Transformer Windings' RLC Parameters Calculation and Lightning Impulse Voltage Distribution Simulation. *IEEE Trans. Magn.* **2016**, *52*.10.1109/TMAG.2015.2481004. [CrossRef]
6. Shibuya, Y.; Fujita, S.; Tamaki, E. Analysis of very fast transients in transformers. *IEE Proc. Gener. Transm. Distrib.* **2002**, *148*, 377–383. [CrossRef]
7. Jurisic, B.; Uglesic, I.; Xemard, A.; Paladian, F. High frequency transformer model derived from limited information about the transformer geometry. *Int. J. Electr. Power Energy Syst.* **2018**, *94*, 300–310. [CrossRef]
8. Villanueva-Ramírez, J.M.; Gómez, P.; Espino-Cortés, F.P.; Nájera, G. Implementation of time domain transformer winding models for fast transient analysis using Simulink. *Int. J. Electr. Power Energy Syst.* **2014**, *61*, 118–126. [CrossRef]
9. Florkowski, M.; Furgał, J.; Kuniewski, M. Propagation of Overvoltages in the Form of Impulse, Chopped and Oscillating Waveforms in Transformer Windings—Time and Frequency Domain Approach. *Energies* **2020**, *13*, 304. [CrossRef]
10. Furgał, J.; Kuniewski, M.; Pająk, P. Analysis of Internal Overvoltages in Transformer Windings during Transients in Electrical Networks. *Energies* **2020**, *13*, 2644. [CrossRef]
11. Trkulja, B.; Drandić, A.; Milardić, V.; Župan, T.; Žiger, I.; Filipović-Grčić, D. Lightning impulse voltage distribution over voltage transformer windings—Simulation and measurement. *Electr. Power Syst. Res.* **2017**, *147*, 185–191. [CrossRef]
12. Lamedica, R.; Pompili, M.; Sangiovanni, S.; Calcara, L.; Ruvio, A.; Cauzillo, B.A. Transient-state analysis of MV instrument transformers. *Electr. Power Syst. Res.* **2019**, *168*, 162–168. [CrossRef]
13. Gunawardana, M.; Fattal, F.; Kordi, B. Very Fast Transient Analysis of Transformer Winding Using Axial Multiconductor Transmission Line Theory and Finite Element Method. *IEEE Trans. Power Deliv.* **2019**, *34*, 1948–1956. [CrossRef]
14. Aghmasheh, R.; Rashtchi, V.; Rahimpour, E. Gray Box Modeling of Power Transformer Windings for Transient Studies. *IEEE Trans. Power Deliv.* **2017**, *32*, 2350–2359. [CrossRef]

15. Filipović-Grčić, D.; Filipović-Grčić, B.; Uglešić, I. High-Frequency Model of the Power Transformer Based on Frequency-Response Measurements. *IEEE Trans. Power Deliv.* **2015**, *30*, 34–42. [CrossRef]

16. Luna López, Z.; Gómez, P.; Espino-Cortés, F.P.; Peña-Rivero, R. Modeling of Transformer Windings for Fast Transient Studies: Experimental Validation and Performance Comparison. *IEEE Trans. Power Deliv.* **2017**, *32*, 1852–1860. [CrossRef]

17. Dommel, H.W. Digital Computer Solution of Electromagnetic Transients in Single-and Multiphase Networks. *IEEE Trans. Power Appar. Syst.* **1969**, *88* , 388–399. [CrossRef]

18. Okuyama, K.; Hosoya, T. A calculation method for impulse voltage distribution and transferred voltage in transformer windings. *IEEE Trans. Power Appar. Syst.* **1978**, *97* , 930–939. [CrossRef]

19. Bebendorf, M. Approximation of boundary element matrices. *Numer. Math.* **2000**, *86*, 565–589. [CrossRef]

20. Bebendorf, M.; Rjasanow, S. Adaptive low-rank approximation of collocation matrices. *Computing* **2003**, *70*, 1–24. [CrossRef]

21. Rjasanow, S. Adaptive Cross Approximation of Dense Matrices. In Proceedings of the International Association for Boundary Element Methods, Austin, TX, USA, 28 May 2002; pp. 28–30.

22. Župan, T.; Štih, Ž.; Trkulja, B. Fast and Precise Method for Inductance Calculation of Coaxial Circular Coils with Rectangular Cross Section Using the One-Dimensional Integration of Elementary Functions Applicable to Superconducting Magnets. *IEEE Trans. Appl. Supercond.* **2014**, *24*. [CrossRef]

23. Trkulja, B.; Štih, Ž.; Župan, T. Calculation of low frequency electric fields of complex power system facilities. *Int. Rev. Electr. Eng.* **2011**, *6*, 1024–1029.

24. Singer, H.; Steinbigler, H.; Weiss, P. A charge simulation method for the calculation of high voltage fields. *IEEE Trans. Power Appar. Syst.* **1974**, *93*, 1660–1668. [CrossRef]

25. Drandić, A.; Trkulja, B. Computation of electric field inside substations with boundary element methods and adaptive cross approximation. *Eng. Anal. Bound. Elem.* **2018**, *91*, 1–6. [CrossRef]

26. Ostrowski, J.; Andjelic, Z.; Bebendorf, M.; Cranganu-Cretu, B.; Smajic, J. Fast BEM-solution of Laplace problems with H-matrices and ACA. *IEEE Trans. Magn.* **2006**, *42*, 627–630. [CrossRef]

27. Jiang, Z.; Chen, H.; Wan, T.; Ouyang, Y.; Qiao, X.; Lu, X. Application of multilevel directional adaptive cross approximation technique for electromagnetic problems. *Eng. Anal. Bound. Elem.* **2017**, *85*, 111–115. [CrossRef]

28. Kurz, S.; Rain, O.; Rjasanow, S. Application of the adaptive cross approximation technique for the coupled BE-FE solution of symmetric electromagnetic problems. *Comput. Mech.* **2003**, *32*, 423–429. [CrossRef]

29. Wei, X.; Chen, B.; Chen, S.; Yin, S. An ACA-SBM for some 2D steady-state heat conduction problems. *Eng. Anal. Bound. Elem.* **2016**, *71*, 101–111. [CrossRef]

30. Drandić, A.; Trkulja, B. Transformer capacitance matrix computation using 3D boundary element method and adaptive cross approximation. *Int. J. Numer. Model. Electron. Netw. Devices Fields* **2019**, *33*, e2669. [CrossRef]

31. Drandić, A.; Trkulja, B. Fast computation of electric field and capacitance matrix of transformer windings with boundary element method and adaptive cross approximation. *IET Electr. Power Appl.* **2019**, *13*, 1422–1427. [CrossRef]

32. Zhao, K.; Vouvakis, M.N.; Lee, J.F. The adaptive cross approximation algorithm for accelerated method of moments computations of EMC problems. *IEEE Trans. Electromagn. Compat.* **2005**, *47*, 763–773. [CrossRef]

33. Tamayo, J.M.; Heldring, A.; Rius, J.M. Multilevel adaptive cross approximation (MLACA). *IEEE Trans. Antennas Propag.* **2011**, *59*, 4600–4608. [CrossRef]

34. Saad, Y.; Schultz, M.H. GMRES: A Generalized Minimal Residual Algorithm for Solving Nonsymmetric Linear Systems. *SIAM J. Sci. Stat. Comput.* **1986**, *7*, 856–869. [CrossRef]